Developmental genetics of corolla tube formation: role of the tasiRNA-ARF pathway

Baoqing Ding[1*], Rui Xia[2,3], Vandana Gurung[1], Janelle M. Sagawa[1], Lauren E. Stanley[1], Matthew Strobel[1], Qiaoshan Lin[1], Pamela K. Diggle[1], Blake C. Meyers[3,4], Yao-Wu Yuan[1,5,*]

[1]Department of Ecology and Evolutionary Biology, University of Connecticut, Storrs, CT 06269, USA

[2]State Key Laboratory for Conservation and Utilization of Subtropical Agro-Bioresources, South China Agricultural University, Guangzhou, Guangdong 510642, China

[3]Donald Danforth Plant Science Center, St. Louis, MO 63132, USA

[4]Division of Plant Sciences, University of Missouri–Columbia, Columbia, MO 65211, USA

[5]Institute for Systems Genomics, University of Connecticut, Storrs 06269, USA

*Corresponding authors:

Baoqing Ding, Department of Ecology and Evolutionary Biology, University of Connecticut, Storrs, CT, 06269; Phone: 860-486-4154; Email: ding.baoqing@gmail.com

Yao-Wu Yuan, Department of Ecology and Evolutionary Biology, University of Connecticut, Storrs, CT, 06269; Phone: 860-486-3469 Email: yuan.colreeze@gmail.com

Abstract

More than 80,000 angiosperm species produce flowers with petals fused into a corolla tube (i.e., sympetalous flowers). As an important element of the tremendous diversity of flower morphology, the corolla tube plays a critical role in many specialized interactions between plants and animal pollinators (e.g., beeflies, hawkmoths, hummingbirds, nectar bats), which in turn drives rapid plant speciation. Despite its clear significance in plant reproduction and evolution, the corolla tube remains one of the least understood plant structures from a developmental genetics perspective. Through mutant analyses and transgenic experiments, here we show that the tasiRNA-ARF pathway is required for corolla tube formation in the monkeyflower species *Mimulus lewisii*. Loss-of-function mutations in the *M. lewisii* orthologs of *ARGONAUTE7* and *SUPPRESSOR OF GENE SILENCING 3* cause a dramatic decrease in abundance of *TAS3*-derived small RNAs and a moderate up-regulation of *AUXIN RESPONSE FACTOR 3* (*ARF3*) and *ARF4*, which lead to inhibition of lateral expansion of the bases of petal primordia and complete arrest of the upward growth of the inter-primordial regions, resulting in unfused corollas. Importantly, by integrating the molecular and phenotypic analyses of the tasiRNA-ARF pathway in *Mimulus* with historical insights from morphological and anatomical studies in various sympetalous species, we propose a new conceptual model for the developmental genetic control of corolla tube formation. This model offers logical connections among the sporadic previous reports of corolla tube mutants in other species and makes clear predictions that can be readily tested using the *Mimulus* system.

Introduction

About one third of the ~275,000 angiosperm species produce flowers with petals fused into a corolla tube (i.e., sympetalous), forming a protective enclosure of nectaries and reproductive organs. Corolla tubes have evolved multiple times independently across the angiosperm tree of life (*1*), most notably in the common ancestor of the Asterids, a clade containing more than 80,000 species (*2*). Subsequent elaboration in length, width, and curvature has led to a great variety of corolla tube shapes that enabled asterid species to exploit many specialized pollinator groups (e.g., beeflies, hawkmoths, hummingbirds, nectar bats), which in turn drives rapid plant speciation (*3*-*6*). As such, the corolla tube

has long been considered a key morphological innovation that contributed to the radiation of the Asterids (*1*). Despite its critical importance in the reproductive success and evolution of such a large number of species, the corolla tube remains one of the least understood plant structures from a developmental genetics perspective (*7*, *8*) .

Historically, corolla tube formation has been the subject of extensive morphological and anatomical studies (*9-19*). In particular, numerous studies have described the detailed ontogenetic process of corolla tube development in one subgroup of the asterid clade, the Lamiids, which contains some classical plant genetic model systems such as snapdragon (*Antirrhinum*), petunia (*Petunia*), and morning glory (*Ipomoea*) (*11-16, 20-22*). A common theme emerging from these studies is that during the early stage of petal development, petal primordia are initiated separately, followed by rapid extension of the petal bases toward the inter-primordial regions, which also grow coordinately, causing congenital "fusion" of the petal primordia and formation of the corolla tube. Little is known, however, about the genetic control of this early-phase lateral extension or the nature of the coordinated inter-primordial growth.

To date only a few genes have been implicated in corolla tube formation. Loss-of-function alleles of the *FEATHERED* gene in Japanese morning glory (*Ipomoea nil*) and the *MAEWEST* gene in petunia (*Petunia x hybrida*), both generated by transposon insertions, result in unfused corollas (*23*, *24*). *FEATHERED* and *MAEWEST* encode KANADI and WOX transcription factors, and their *Arabidopsis* orthologs are *KANADI1* and *WOX1*, respectively. In addition, ectopic expression of the *Arabidopsis* TCP5 protein fused with a repressor motif in *Ipomoea* also disrupted corolla tube formation (*25*). However, whether the endogenous *TCP5* ortholog in *Ipomoea* is involved in corolla tube development is unclear. More recently, it was reported that transient knock-down of the *Petunia* NAC-transcription factors *NAM* and *NH16* via virus-induced gene silencing (VIGS) also caused decreased petal fusion (*26*), but the interpretation of this result was confounded by the observation that occasional flowers produced on the "escape shoots" of the loss-of-function *nam* mutants have normal corolla tubes (*27*). The fact that these genes were characterized from different plant systems and through different methods (transposon insertion alleles, heterologous expression of chimeric repressor, and VIGS)

makes it challenging to interpret their genetic relationships and their precise functional roles in corolla tube formation.

One way to overcome this problem is to systematically analyze corolla tube mutants in a single model system. To this end, we have employed a new genetic model system, the monkeyflower species *Mimulus lewisii*, mainly for its ease in chemical mutagenesis and *Agrobacterium*-mediated *in planta* transformation (*28, 29*). *M. lewisii* is a typical bumblebee-pollinated species with a conspicuous corolla tube (Fig. 1A). Through ethyl methanesulfonate (EMS) mutagenesis, we have generated a dozen recessive mutants (named *flayed*) with split corolla tubes. Here we report the characterization of one group of mutants, caused by loss-of-function mutations in two genes that are required for the biogenesis of *trans*-acting short interfering RNAs (tasiRNAs).

Among the tasiRNA loci characterized to date, *TAS3* is the most widely conserved, found in virtually all land plants (*30*). *TAS3* transcript bears two binding sites for miR390, which triggers the production of phased tasiRNAs, including the highly conserved "tasiARF" that targets *AUXIN RESPONSE FACTOR 3* (*ARF3*) and *ARF4* (*31, 32*). This tasiRNA-ARF regulatory module has been shown to play a critical role in leaf polarity and blade expansion (i.e., lamina growth) in both eudicots (*33-38*) and monocots (*39-41*). Consistent with previous studies, here we demonstrate that in the *M. lewisii* mutants, *TAS3*-derived tasiRNAs decrease dramatically in abundance and *MlARF3* and *MlARF4* expression are upregulated. Importantly, we show that malfunction of the tasiRNA-ARF pathway in the *M. lewisii* mutants impedes the early lateral expansion of the petal primordium bases and the coordinated inter-primordial growth, consequently preventing the congenital fusion of the petal primordia. Integrating our molecular and phenotypic analyses of the tasiRNA-ARF pathway in *Mimulus* with historical insights from morphological and anatomical studies of various sympetalous species, we propose a new conceptual model for the genetic control of corolla tube formation, which offers logical connections among the sporadic previous reports of corolla tube mutants and makes clear predictions that can be readily tested using the *Mimulus* system.

Results and Discussion

Phenotypic Characterization of the *flayed1* and *flayed2* Mutants. Three of the recessive mutants recovered from EMS mutagenesis using the inbred line LF10, *flayed1-flayed3*, are morphologically indistinguishable. Pair-wise crosses suggested that they belong to two complementation groups, *flayed1* and *flayed2* (*flayed3* is allelic to *flayed2*) (Fig. 1B and C). In addition to having unfused petals, these mutants display carpel fusion defects, with phenotypes varying from flower to flower within the same plant. Most mutant flowers have two fused carpels, as in the wild-type, but have partially split stigmas with more than two lobes (Fig. 1E). Less frequently there are flowers with two almost completely separate styles. The length of mutant pistils is also reduced compared to the wild-type (Fig. 1E). No obvious phenotypes were observed in the stamens of these mutants.

Another notable feature of the *flayed1/2* mutants is the reduced width of lateral organs. The dorsal and lateral petals show ~30% decrease in width compared to the wild-type, and the ventral petal shows ~37% decrease (Fig. 1F; Table S1). Leaf width is also substantially reduced (by ~40%) in the mutants, but leaf length is unaffected (Fig. 1G and H; Table S1). To determine whether the reduction in petal width is due to change in cell number, cell size, or both, we measured the width of abaxial epidermal cells of the dorsal petal lobe for both the wild-type and the *flayed2* mutant. Because the petal lobe abaxial epidermal cells are irregularly shaped (Fig. 1I), the width measurements were done on five contiguous cells to account for the variation among individual cells within the same sample. No significant difference in cell width was found between the wild-type and *flayed2* (Fig. 1J), which suggests that the difference in petal width between the mutant and the wild-type is primarily due to difference in cell number (i.e., number of cell divisions).

Unlike the morning glory mutant *feathered* (*23*) or the petunia mutant *maewest* (*24*), *flayed1/2* do not show any defects in tissue adaxial-abaxial polarity. Instead, the *flayed1/2* mutants closely resemble the petunia mutant *choripetala suzaane* (*chsu*), which also has a split corolla tube, variable carpel fusion defects, and narrower leaf with normal adaxial/abaxial polarity. Unfortunately, the molecular identity of *CHSU* is still unknown.

***FLAYED1* and *FLAYED2* Are the Orthologs of Arabidopsis *AGO7* and *SGS3*, Respectively.** To identify the causal genes of *flayed1* and *flayed2*, we analyzed each mutant using a genomic approach that combines the advantages of bulk segregant analysis and comparison of single nucleotide polymorphism (SNP) profiles between multiple EMS mutants (*Materials and Methods*), as demonstrated in a previous study (*42*). We narrowed the causal mutation of *flayed1* and *flayed2* down to 38 and 19 candidate SNPs, respectively (Table S2 and S3). The vast majority of these SNPs locate in non-coding, repetitive sequences, with only two or three mutations resulting in amino acid changes in each mutant (Table S2 and S3). Notably, in both *flayed1* and *flayed2*, there is one mutation leading to a premature stop codon, in the ortholog of Arabidopsis *ARGONAUTE7* (*AGO7*) and *SUPPRESSOR OF GENE SILENCING 3* (*SGS3*), respectively (Fig. 2A and B; Table S2 and S3). *AGO7* and *SGS3* are part of the same tasiRNA biogenesis pathway (*43-45*), which would explain the indistinguishable mutant phenotypes of *flayed1* and *flayed2*. Furthermore, sequencing the coding DNA (CDS) of *MlSGS3* in *flayed3*, which is allelic to *flayed2*, revealed an independent mutation that also leads to a premature stop codon (Fig. 2B). Together, these results suggested that *MlAGO7* and *MlSGS3* were the most promising candidate genes for *FLAYED1* and *FLAYED2*, respectively.

To verify gene identities, full-length CDS of *MlAGO7* and *MlSGS3* were introduced to the *flayed1* and *flayed2* mutant background, respectively, driven by the cauliflower mosaic virus 35S promoter. Among the 29 independent *35S:MlAGO7* lines in the *flayed1* background, 13 showed a fully rescued phenotype that is indistinguishable from the wild-type; four lines showed a partially rescued phenotype, with petal width increased to wild-type level but the petals remained unfused (Fig. 2C). Similarly, six of the 18 *MlSGS3* over-expression lines in the *flayed2* background displayed a fully rescued phenotype and two displayed a partially rescued phenotype (Fig. 2D). qRT-PCR assessment of *MlAGO7* and *MlSGS3* expression in 5-mm floral buds showed that, in the fully rescued lines, expression levels of the transgenes are 4~64-fold higher than those of the corresponding endogenous genes (Fig. S1). These results confirmed that *MlAGO7* and *MlSGS3* are indeed the causal genes underlying *flayed1* and *flayed2*, respectively.

Knowing the causal genes and mutations allowed direct genotyping of a "*flayed1* x *flayed2*" F_2 population to identify *flayed1 flayed2* double mutants, which are phenotypically indistinguishable from the single mutants (Fig. 1D, F, G, H). This further indicates that *MlAGO7* and *MlSGS3* function in the same genetic pathway in *Mimulus*, as expected.

The *flayed1/2* Phenotypes Are Primarily Mediated Through the tasiRNA-ARF Pathway. Because *AGO7* and *SGS3* are necessary components of the miR390-*TAS3-ARF* pathway (Fig. 3A), and the highly conserved, *TAS3*-derived tasiARFs are known to play a critical role in leaf polarity and lamina growth by repressing *ARF3/4* expression (*33-41*), we hypothesized that the *flayed1/2* phenotypes (e.g., reduced width of lateral organs) are primarily mediated through the tasiRNA-ARF pathway. This hypothesis makes three clear predictions: (**i**) The abundance of *TAS3*-derived small RNAs, including tasiARFs, should be much lower in the mutants compared to the wild-type; (**ii**) The *M. lewisii* orthologs of *ARF3/4* should be upregulated in the mutants; and, (**iii**) Artificial upregulation of the *M. lewisii ARF3/4* orthologs in the wild-type background should recapitulate the *flayed1/2* phenotypes.

To test the first prediction, we sequenced the total small RNA pool from young floral buds (5-mm) of the wild-type, *flayed1*, and *flayed 2*. Like most other angiosperms, *M. lewisii* has two kinds of *TAS3* genes (each represented by only a single copy in the *M. lewisii* genome): *TAS3S* contains a single, centrally located tasiARF, whereas *TAS3L* contains two tandem tasiARFs (*30*; Fig. S2). No *TAS3S*-derived small RNAs were detected in any of the sequenced samples, suggesting that the *TAS3S* gene is not expressed. *TAS3L*-derived small RNAs were detected at the level of ~600 per million reads in the wild-type, but decreased >50-fold in both *flayed1* and *flayed2* (Fig. 3B). In particular, the tasiARFs were almost entirely absent from the mutant samples (Fig. 3B). These results confirmed the first prediction.

To test the second prediction, we first searched the *M. lewisii* genome for *ARF3/4* homologs and found a single ortholog for each of the two genes. Similar to *ARF3/4* in other species, both *MlARF3* and *MlARF4* have two binding sites with sequences complementary to tasiARF (Fig. 4A and B). qRT-PCR measurements in 5-mm floral

buds showed that in the single and double mutants, *MlARF3* was up-regulated by 1.7~2.5-fold and *MlARF4* was up-regulated by 2.7~3.7-fold (Fig. 4C). This moderate up-regulation of *ARF3/ARF4* in the *ago7* and *sgs3* mutant backgrounds is very similar to previous reports in *Arabidopsis* (Garcia et al., 2006; Hunter et al., 2006), supporting the role of tasiARF in fine-tuning *ARF3/4* expression level.

To test the third prediction, we transformed the wild-type with a tasiARF-insensitive version of *MlARF3* (*mMlARF3*) and *MlARF4* (*mMlARF4*) with several synonymous substitutions at the tasiARF binding sites (Fig. 4A and B), driven by the 35S promoter. We obtained seven independent *35S:mMlARF3* and 14 *35S:mMlARF4* lines. In each case, only two transgenic lines showed obvious phenotypes: their leaves are very similar to the *flayed1/2* mutants (i.e., narrower than the wild-type) and corollas are partially split (indicated by the red arrow heads in Fig. 4D and E). qRT-PCR experiments on 5-mm floral buds of the transgenic lines with even the strongest phenotypes showed only moderate overexpression of *MlARF3/4* relative to the wild-type (2~4-fold, Fig. S3A and B). Examination of two random *35S:mMlARF4* lines without obvious phenotypes showed no increase in expression level of *MlARF4* (Fig. S2C). The lack of *35S:mMlARF3/4* lines with strong transgene expression is in contrast to ectopic expression of *MlAGO7* and *MlSGS3* (Fig. S1) as well as pigment-related transcription factors in *M. lewisii* (*46*, *47*), where the same 35S promoter could readily drive transgene expression level >10-fold higher than that of the endogenous genes. One possible explanation for this observation is that transgenic lines with very strong *ARF3/4* expression in *M. lewisii* are seedling lethal, as implicated by similar experiments in tomato (*37*). Nevertheless, our results show that a moderate up-regulation of *MlARF3/4* can indeed fully recapitulate the leaf phenotype and partially recapitulate the flower phenotype of the *flayed1/2* mutants. Furthermore, a double transgenic line derived from a cross between the strongest *35S:mMlARF3* line and *35S:mMlARF4* line showed dramatic petal fusion defects (Fig. 4F), more closely resembling the *flayed1/2* mutants than the single transgenic lines. This indicates that *MlARF3* and *MlARF4* may act synergistically in regulating corolla tube formation. Taken together, our results from transgenic manipulation of the *MlARF3/4* expression levels suggest that the *flayed1/2* phenotypes

(narrow leaf and split corolla tube) are primarily mediated by the up-regulation of *MlARF3/4*.

The tasiRNA-ARF Pathway Is Required for Preferential Lateral Expansion of the Bases of Petal Primordia and Coordinated Growth of Inter-primordial Regions. To understand how malfunction of the tasiRNA-ARF pathway affects corolla tube formation in *M. lewisii*, we have studied floral organogenesis in the wild-type and the *flayed2* mutant using scanning electron microscopy. Like other species in the Lamiid clade (e.g., snapdragon, petunia, morning glory), *M. lewisii* petals are initiated as five separate primordia (Fig. 5A). Petal development lags behind stamens in the early stages (Fig. 5B and C), but by the time the corolla reaches ~0.5 mm in diameter (Fig. 5D), petal development progresses rapidly and soon the stamens are found enclosed in the corolla (Fig. 5E-H). The developmental stage from 0.3 to 0.4 mm (corolla diameter) is critical for corolla tube formation: during this stage, the bases of the petal primordia quickly expand laterally (to a conspicuously greater extent than the upper portion of the petal primordia; Fig. 5M), and the inter-primordial regions also grow coordinately, connecting the initially separate petal primordia. Floral organogenesis of *flayed2* is very similar to that of the wild-type at the early stages (before the corolla reaches 0.3 mm in diameter; Fig. 5I). However, during the critical period (0.3~0.4 mm), there is no preferential lateral expansion at the bases of the petal primordia, manifested as the truncate shape of the petal primordium base (Fig. 5N), in contrast to the semi-circle shape of the wild-type (Fig. 5M). Notably, growth of the inter-primordial regions is also arrested in *flayed2*, leading to a gap between two adjacent petal primordia (Fig. 5J-L and indicated by the asterisk in Fig. 5N).

Given that disruption of tasiRNA biogenesis and the consequent up-regulation of *ARF3/4* have been shown to cause reduced lamina growth of lateral organs in multiple plant species (*36-38, 41*), it is not surprising to observe reduced lateral expansion at the bases of the petal primordia in *flayed2* compared to the wild-type (Fig. 5M and N). But how does this relate to the arrest of *upward* growth of the inter-primordial regions?

In a series of careful anatomical studies of various taxa in the Asterid clade, Nishino (*12-15*) recognized that the “co-operation” between the marginal meristem

activities of the base of the petal primordia and the upward growth of the inter-primordial regions plays a pivotal role in corolla tube formation, although the nature of this "co-operation" was unclear. In light of this earlier insight, we interpreted the *flayed2* phenotype as follows: in the wild-type there is molecular signaling from the marginal meristematic cells at the bases of the petal primordia to the inter-primordial cells, stimulating the latter to grow upward coordinately (i.e., the nature of the "co-operation" is molecular signaling between the two regions). In the *flayed2* mutant, this molecular signaling is disrupted, causing a complete arrest of the upward growth of the inter-primordial regions. An obvious candidate for this putative signal is the phytohormone auxin, which is known to promote localized tissue outgrowth and meanwhile suppress organ boundary genes such as *CUP-SHAPED COTYLEDON 1* (*CUC1*) *and CUC2* in Arabidopsis (*48*).

A Conceptual Model for the Genetic Control of Corolla Tube Formation: Two recent attempts of building a conceptual framework for floral organ fusion in general (*7*) or petal fusion in particular (*8*) both emphasized the genetic regulatory network underlying organ boundary formation and maintenance. The rationale for such emphasis was explicitly stated by Specht and Howarth (*7*): "*fusion as a process may more accurately be defined as a lack of organ separation*". While these attempts represent an important step towards a mechanistic understanding of the developmental process of corolla tube formation, to some degree they have neglected the insight provided by earlier morphological and anatomical studies (i.e., the importance of the "co-operation" between the rapid lateral expansion of the petal primordium bases and the upward growth of the inter-primordial regions), and have not provided a logical integration of the sporadic reports of corolla tube mutants (*23*, *24*, *49*).

Building on the historical insight from anatomical studies and our molecular and phenotypic analyses of the tasiRNA-ARF pathway in *Mimulus*, we propose a new conceptual model that offers logical connections among the sporadic previous reports on the genetic control of corolla tube formation (Fig. 6). This model consists of three inter-connected modules. At the heart of the model is the molecular signaling from the marginal meristematic cells at the base of the petal primordia to the inter-primordial cells, providing a molecular explanation for the "co-operation" between the petal primordia and

inter-primordial regions observed in anatomical studies. Upstream of this core module is the genetic regulatory network responsible for lateral expansion of the petal primordium base, which is required for initiation of the molecular signaling. Downstream of this core module lie the organ boundary genes that would suppress localized tissue growth if not repressed by the molecular signal coming from the petal primordia.

This model can readily explain the phenotypes of loss-of-function mutations in the morning glory *FEATHERED* gene and the petunia *MAEWEST* gene, which encode KANADI and WOX transcription factors, respectively (*23*, *24*). Together with the tasiRNA-ARF pathway, these transcription factors are part of the genetic network regulating leaf adaxial-abaxial polarity and lamina growth (*50*-*52*). According to our model, disrupting this genetic regulatory network is expected to impede lateral expansion of the petal primordia, as in the *flayed2* mutant (Fig. 5N), and consequently break the signaling from the petal primordia to the inter-primordial cells, resulting in unfused petals. A less dramatic corolla tube phenotype was also observed in the snapdragon *graminifolia* mutant, with fusion defect restricted to the two dorsal petals (*49*). *GRAMINIFOLIA* encodes a YABBY transcription factor (*49*), another component of the leaf polarity/lamina growth genetic network. This example further highlights the importance of the "lamina growth" module in the model (Fig. 6).

Our model also provides a plausible explanation for the petal fusion defects observed when a chimeric repressor of AtTCP5 was over-expressed in the Japanese morning glory (*25*). Chimeric repressors of CIN-like TCP transcription factors, including TCP5 in Arabidopsis, are known to activate organ boundary genes such as *CUC1/2* (*53*). Ectopic activation of *CUC1/2* is expected to prevent the upward growth of the inter-primoridial regions (i.e., boundary between adjacent petal primordia). Also consistent with the "organ boundary" module (Fig. 6) is a recent observation in snapdragon — the expression of the *CUC* ortholog, *CUPULIFORMIS*, is cleared from the inter-primordial regions shortly after petal initiation but later is reactivated in the sinuses between adjacent corolla lobes (*54*). Through computational modeling, Rebocho et al. (*54*) showed that this "gap" of *CUPULIFORMIS* expression (between the base of the corolla and the sinuses) is necessary for corolla tube formation.

In addition to explaining these previous observations, our model predicts that transgenic manipulation of other components of the leaf polarity/lamina growth network (e.g., *AS1*, *AS2*, *HD-ZIPIII*) (*50-52*) or ectopic expression of organ boundary genes (e.g., *CUC*, *ORGAN BOUNDARY1*, *JAGGED LATERAL ORGAN*) (*55-57*) in sympetalous species may also result in unfused corollas; it also predicts that misregulation of the molecular signaling, as proposed in the core module (Fig. 6), in transgenic or mutant plants should produce defective corolla tubes. If the putative signal is indeed auxin, regulation of polarized auxin transport within and between petal primordia will be key to understanding corolla tube formation. The availability of multiple corolla tube mutants, the ease of bulk segregant analysis to identify mutant genes, and the amenability of *Agrobacterium*-mediated *in planta* transformation make *Mimulus* a favorable system to test these predictions and to dissect the detailed molecular mechanisms and developmental process of corolla tube formation.

Materials and Methods

Plant Materials and Growth Conditions. EMS mutagenesis was performed using the *Mimulus lewisii* Pursh inbred line LF10 as described (*28*). Another inbred line SL9 was used to generate the "*flayed* x SL9" F_2 populations. Plants were grown in the University of Connecticut research greenhouses under natural light supplemented with sodium vapor lamps, ensuring a 16-hr day length.

Phenotypic Characterization. To quantify phenotypic differences between the mutants and wild-type, we measured the widths of the dorsal, ventral, and lateral petals using a digital caliper. We also measured the lengths and widths of the fourth leaf (the largest leaf) of mature plants. To further evaluate whether the width difference is due to change in cell number, cell size or both, width of the abaxial epidermal cells of the dorsal petal lobe was measured following a previously described procedure (*58*).

Genomic Analyses for Causal Gene Identification. To identify causal genes underlying *flayed1* and *flayed2*, we employed a hybrid strategy that combines the advantages of bulk segregant analysis and genome comparisons between multiple EMS mutants, as

described previously (*42*). Briefly, for each mutant an F_2 population was produced by crossing the homozygous mutant (generated in the LF10 background) and the mapping line SL9. DNA samples from 96 F_2 segregants displaying the mutant phenotype (i.e., homozygous for the causal mutation) were pooled with equal representation. A small-insert library was then prepared for the pooled sample and was sequenced using an Illumina HiSeq 2000 platform at the University of North Carolina High Throughput Sequencing Facility. About 213 and 448 million 100-bp paired-end reads were generated for *flayed1* and *flayed2*, respectively.

The short reads were mapped to the LF10 genome assembly version 1.8 (http://monkeyflower.uconn.edu/resources/) using CLC Genomics Workbench 7.0 (Qiagen, Valencia, CA). The causal mutation should be: (**i**) homozygous for the pooled sample (i.e., 100% SNP frequency in the "F_2 reads – LF10 genome" alignment); and (**ii**) unique to each mutant (i.e., any shared 100% SNPs between mutants are most likely due to assembly error in the reference genome or non-specific mapping of repetitive sequences). After comparisons to the SNP profiles of previously published mutants, *guideless* (*59*), *rcp1* (*47*), *act1-D* (*58*), and *rcp2* (*60*), we narrowed the causal mutation to 39 and 19 candidate SNPs for *flayed1* and *flayed2*, respectively (Fig. S3).

Small RNA Sequencing and Analyses. For small RNA sequencing, total RNA was first extracted using the Spectrum Plant Total RNA Kit (Sigma-Aldrich) from 5-mm floral buds of LF10, *flayed1*, and *flayed2* (two biological replicates for each genotype). Small RNA libraries were then constructed using the TruSeq Small RNA Sample Preparation Kits (Illumina), with the total RNA as starting material. The libraries were sequenced on an Illumina HiSeq 2500 at the Delaware Biotechnology Institute (Newark, DE). Small RNA reads were quality-controlled and adaptor-trimmed before calculating tasiRNA abundance, as described in Xia et al. (*30*).

Quantitative RT-PCR. RNA extraction and cDNA synthesis were as previously described (*29*). cDNA samples were diluted 10-fold before quantitative reverse transcriptase PCR (qRT-PCR). All qRT-PCRs were performed using iQ SYBR Green Supermix (Bio-Rad) in a CFX96 Touch Real-Time PCR Detection System (Bio-Rad).

Samples were amplified for 40 cycles of 95 ºC for 15 s and 60 ºC for 30 s. Amplification efficiencies for each primer pair were determined using critical threshold values obtained from a dilution series (1:4, 1:8, 1:16, 1:32) of pooled cDNA. *MlUBC* was used as a reference gene as described (*29*). Primers used for qRT-PCR are listed in Table S4.

Plasmid Construction and Plant Transformation. To generate the *35S:MlAGO7* and *35S:MlSGS3* constructs for the rescue experiments, we first amplified the full-length CDS of *MlAGO7* and *MlSGS3* from the wild-type LF10 cDNA using the Phusion enzyme (NEB, Ipswich, MA). For each gene, the amplified fragment was cloned into the pENTR/D-TOPO vector (Invitrogen) and then a linear fragment containing the CDS flanked by the attL1 and attL2 sites was amplified using M13 primers. This linear fragment was subsequently recombined into the Gateway vector pEarleyGate 100 (*61*), which drives transgene expression by the CaMV *35S* promoter.
To generate the *35S:mMlARF3/4* constructs, CDS of insensitive forms of *MlARF3* (*mARF3*) and *MlARF4* (*mARF4*) that carries synonymous substitutions in the two tasiRNA recognition sites were synthesized by GenScript (NJ, USA) and then cloned into the pEarleyGate 100 destination vector as described for the *35S:MlAGO7* and *35S:MlSGS3* constructs. All plasmids were verified by sequencing before being transformed into *Agrobacterum tumefaciens* strain GV3101 for subsequent plant transformation, as described in Yuan et al. (*29*). Primers used for plasmid construction and sequencing are listed in Table S5.

Scanning Electron Microscopy. Flower buds were fixed overnight in Formalin-Acetic-Alcohol (FAA) at 4°C, dehydrated for 30 min through a 50%, 60%, 70%, 95%, and 100% alcohol series. Samples were then critical-point dried, mounted, and sputter coated before being observed using a NOVA NanoSEM with Oxford EDX at 35 kV at UConn's Bioscience Electron Microscopy Laboratory.

Author Contributions

B.D. designed the study, performed most of the phenotypic characterization and functional experiments, analyzed and interpreted the data, and drafted the manuscript.

R.X. and B.C.M. acquired and analyzed small RNA data. V.G. and P.K.D. acquired and interpreted the SEM images. J.M.S., L.E.S., and M.S. contributed to the transgenic experiments. Q.L. interpreted the data and illustrated the model (Figure 6). Y.W.Y. conceived and designed the project, analyzed and interpreted the data, and drafted the manuscript. All authors reviewed the manuscript.

Acknowledgements

We are grateful to Dr. Toby Bradshaw (University of Washington) for encouragement and initial support for generating the bulk segregant data in his laboratory. We thank Clinton Morse, Matt Opel, and Adam Histen for plant care in the UConn EEB Research Greenhouses. This work was supported by the University of Connecticut start-up funds and an NSF grant (IOS-1558083) to Y-W.Y., and an NSF grant (IOS-1257869) to B.C.M.

Data Availability

Short read data have been deposited in NCBI SRA (BioProject PRJNA423263); small RNA data have been deposited in NCBI GEO (GSE108530); annotated gene sequences have been deposited in GenBank (MG669632- MG669634 and MF084285).

References

1. Endress PK (2011) Evolutionary diversification of the flowers in angiosperms. *Am J Bot* 98:370-396.
2. Schönenberger J, von Balthazar M (2013) Asterids. *Botanical Journal of the Linnean Society* 173:321-324.
3. Muchhala N (2006) Nectar bat stows huge tongue in its rib cage. *Nature* 444:701-702.
4. Hermann K, Kuhlemeier C (2011) The genetic architecture of natural variation in flower morphology. *Curr Opin Plant Biol* 14:60-65.
5. Paudel BR, *et al.* (2015) Out of africa: Evidence of the obligate mutualism between long corolla tubed plant and long-tongued fly in the himalayas. *Ecol. Evol.* 5(22):5240-5251.
6. Lagomarsino LP, Condamine FL, Antonelli A, Mulch A, Davis CC (2016) The abiotic and biotic drivers of rapid diversification in andean bellflowers (campanulaceae). *New Phytologist* 210:1430-1442.
7. Specht CD, Howarth DG (2015) Adaptation in flower form: A comparative evodevo approach. *New Phytologist* 206:74-90.
8. Zhong J, Preston JC (2015) Bridging the gaps: Evolution and development of perianth fusion. *New Phytologist* 208:330-335.
9. Boke NH (1948) Development of the perianth in *Vinca rosea* l. *Am. J. Bot.* 35:413-423.
10. Kaplan DR (1968) Structure and development of the perianth in *Downingia bacigalupii*. *Am. J. Bot.* 55:406-420.
11. Govil CM (1972) Morphological studies in the family Convolvulaceae. *Proceedings of the Indian Academy of Sciences - Section B* 75:271-282.
12. Nishino E (1976) Developmental anatomy of foliage leaves, bracts, calyx and corolla in *Pharbitis nil*. *The botanical magazine* 89:191-209.
13. Nishino E (1978) Corolla tube formation in four species of Solanaceae. *The botanical magazine* 91:263-277.
14. Nishino E (1983a) Corolla tube formation in the Primulaceae and Ericales. *The botanical magazine* 96:319-342.
15. Nishino E (1983b) Corolla tube formation in the Tubiflorae and Gentianales. *The botanical magazine* 96:223-243.
16. Erbar C (1991) Sympetaly—a systematic character. *Bot. Jb* 112:417-451.
17. Erbar C & Leins P (1996) Distribution of the character states "early sympetaly" and "late sympetaly" within the "sympetalae tetracyclicae" and presumably allied groups*. *Plant Biol.* 109:427-440.
18. Verbeke JA (1992) Fusion events during floral morphogenesis. *Annu. Rev. Plant Physiol. Plant Mol. Biol.* 43:583-598.
19. El Ottra JHL, Pirani JR, Endress PK (2013) Fusion within and between whorls of floral organs in Galipeinae (Rutaceae): Structural features and evolutionary implications. *Annals of botany* 111:821-837.
20. Singh V, Jain DK (1979) Floral organogenesis in *Antirrhinum majus* (Scrophulariaceae). *Proceedings of the Indian Academy of Sciences - Section B. Part2, Plant Sciences* 88:183-188.

21. Vincent CA, Coen ES (2004) A temporal and morphological framework for flower development in *Antirrhinum majus*. *Canadian Journal of Botany* 82:681-690.
22. Erbar C, Leins P (2011) Synopsis of some important, non-DNA character states in the asterids with special reference to sympetaly. *Plant Diversity and Evolution* 129:93-123.
23. Iwasaki M, Nitasaka E (2006) The feathered gene is required for polarity establishment in lateral organs especially flowers of the japanese morning glory (*Ipomoea nil*). *Plant Mol. Biol.* 62:913-925.
24. Vandenbussche M, *et al.* (2009) Differential recruitment of wox transcription factors for lateral development and organ fusion in Petunia and Arabidopsis. *The Plant Cell* 21:2269-2283.
25. Ono M, *et al.* (2012) Morphological changes in *Ipomoea nil* using chimeric repressors of Arabidopsis TCP3 and TCP5. *Plant Biotechnology* 29:457-463.
26. Zhong J, Powell S, Preston JC (2016) Organ boundary NAC-domain transcription factors are implicated in the evolution of petal fusion. *Plant Biol.* 18:893-902.
27. Souer E, van Houwelingen A, Kloos D, Mol J, Koes R (1996) The No Apical Meristem gene of Petunia is required for pattern formation in embryos and flowers and is expressed at meristem and primordia boundaries. *Cell* 85:159-170.
28. Owen C, Bradshaw HD (2011) Induced mutations affecting pollinator choice in *Mimulus lewisii* (Phrymaceae). *Arthropod-Plant Interactions* 5:235-244.
29. Yuan Y-W, Sagawa JM, Young RC, Christensen BJ, Bradshaw HD (2013) Genetic dissection of a major anthocyanin QTL contributing to pollinator-mediated reproductive isolation between sister species of *Mimulus*. *Genetics* 194:255-263.
30. Xia R, Xu J, Meyers BC (2017) The emergence, evolution, and diversification of the miR390-TAS3-ARF pathway in land plants. *Plant Cell*.
31. Allen E, Xie Z, Gustafson AM, Carrington JC (2005) microRNA-directed phasing during trans-acting siRNA biogenesis in plants. *Cell* 121:207-221.
32. Axtell MJ, Jan C, Rajagopalan R, Bartel DP (2006) A two-hit trigger for siRNA biogenesis in plants. *Cell* 127:565-577.
33. Hunter C, *et al.* (2006) Trans-acting siRNA-mediated repression of ETTIN and ARF4 regulates heteroblasty in Arabidopsis. *Development* 133:2973-2981.
34. Garcia D, Collier SA, Byrne ME, Martienssen RA (2006) Specification of leaf polarity in Arabidopsis via the trans-acting siRNA pathway. *Curr. Biol.* 16:933-938.
35. Fahlgren N, *et al.* (2006) Regulation of AUXIN RESPONSE FACTOR3 by TAS3 ta-siRNA affects developmental timing and patterning in Arabidopsis. *Curr. Biol.* 16:939-944.
36. Yan J, *et al.* (2010) The reduced leaflet genes encode key components of the trans-acting small interfering RNA pathway and regulate compound leaf and flower development in *Lotus japonicus*. *Plant Physiol* 152:797-807.
37. Yifhar T, *et al.* (2012) Failure of the tomato trans-acting short interfering RNA program to regulate AUXIN RESPONSE FACTOR3 and ARF4 underlies the wiry leaf syndrome. *The Plant Cell* 24:3575-3589.

38. Zhou C, *et al.* (2013) The trans-acting short interfering RNA3 pathway and no apical meristem antagonistically regulate leaf margin development and lateral organ separation, as revealed by analysis of an argonaute7/lobed leaflet1 mutant in *Medicago truncatula*. *The Plant Cell* 25:4845-4862.
39. Nogueira FT, Madi S, Chitwood DH, Juarez MT, Timmermans MC (2007) Two small regulatory RNAs establish opposing fates of a developmental axis. *Genes Dev* 21:750-755.
40. Nagasaki H, *et al.* (2007) The small interfering RNA production pathway is required for shoot meristem initiation in rice. *Proc. Natl. Acad. Sci. U. S. A.* 104:14867-14871.
41. Douglas RN, *et al.* (2010) Ragged seedling2 encodes an ARGONAUTE7-like protein required for mediolateral expansion, but not dorsiventrality, of maize leaves. *The Plant Cell* 22:1441-1451.
42. LaFountain AM, *et al.* (2017) Molecular basis of overdominance at a flower color locus. *G3: Genes|Genomes|Genetics* 7:3947.
43. Peragine A, Yoshikawa M, Wu G, Albrecht HL, Poethig RS (2004) SGS3 and SGS2/SDE1/RDR6 are required for juvenile development and the production of trans-acting siRNAs in Arabidopsis. *Genes & Development* 18:2368-2379.
44. Yoshikawa M, Peragine A, Park MY, Poethig RS (2005) A pathway for the biogenesis of trans-acting siRNAs in Arabidopsis. *Genes Dev.* 19:2164-2175.
45. Chen X (2010) Small RNAs - secrets and surprises of the genome. *Plant J.* 61:941-958.
46. Yuan Y-W, Sagawa JM, Frost L, Vela JP, Bradshaw HD (2014) Transcriptional control of floral anthocyanin pigmentation in monkeyflowers (mimulus). *New Phytologist* 204:1013-1027.
47. Sagawa JM, *et al.* (2015) An R2R3-MYB transcription factor regulates carotenoid pigmentation in *Mimulus lewisii* flowers. *New Phytologist*. 209: 1049-1057
48. Bilsborough GD, *et al.* (2011) Model for the regulation of *Arabidopsis thaliana* leaf margin development. *Proc. Natl. Acad. Sci. U. S. A.* 108:3424-3429.
49. Golz JF, Roccaro M, Kuzoff R, Hudson A (2004) Graminifolia promotes growth and polarity of *Antirrhinum* leaves. *Development* 131:3661-3670.
50. Nakata M, Okada K (2013) The leaf adaxial-abaxial boundary and lamina growth. *Plants* 2:174-202.
51. Tsukaya H (2013) Leaf development. *The Arabidopsis Book* 11:e0163.
52. Kuhlemeier C, Timmermans MCP (2016) The sussex signal: Insights into leaf dorsiventrality. *Development* 143:3230-3237.
53. Koyama T, Furutani M, Tasaka M, Ohme-Takagi M (2007) TCP transcription factors control the morphology of shoot lateral organs via negative regulation of the expression of boundary-specific genes in Arabidopsis. *The Plant Cell* 19:473-484.
54. Rebocho AB, Kennaway JR, Bangham JA, Coen E (2017) Formation and shaping of the Antirrhinum flower through modulation of the cup boundary gene. *Curr. Biol.* 27:2610-2622
55. Aida M, Ishida T, Fukaki H, Fujisawa H, Tasaka M (1997) Genes involved in organ separation in Arabidopsis: An analysis of the cup-shaped cotyledon mutant. *The Plant Cell* 9:841-857.

576 56. Borghi L, Bureau M, Simon R (2007) Arabidopsis JAGGED LATERAL
577 ORGANS is expressed in boundaries and coordinates knox and pin activity. *Plant*
578 *Cell* 19:1795-1808.
579 57. Cho E, Zambryski PC (2011) ORGAN BOUNDARY1 defines a gene expressed
580 at the junction between the shoot apical meristem and lateral organs. *Proc. Natl.*
581 *Acad. Sci. U. S. A.* 108:2154-2159.
582 58. Ding B, *et al.* (2017) A dominant-negative actin mutation alters corolla tube width
583 and pollinator visitation in *Mimulus lewisii*. *New Phytologist* 213:1936-1944.
584 59. Yuan Y-W, Sagawa JM, Di Stilio VS, Bradshaw HD (2013) Bulk segregant
585 analysis of an induced floral mutant identifies a MIXTA-like R2R3 MYB
586 controlling nectar guide formation in *Mimulus lewisii*. *Genetics* 194:523-528.
587 60. Stanley LE, *et al.* (2017) A tetratricopeptide repeat protein regulates carotenoid
588 biosynthesis and chromoplast development in monkeyflowers (mimulus). *bioRxiv*.
589 doi: http://dx.doi.org/10.1101/171249
590 61. Earley KW, et al. (2006) Gateway-compatible vectors for plant functional
591 genomics and proteomics. *Plant J* 45:616-629.

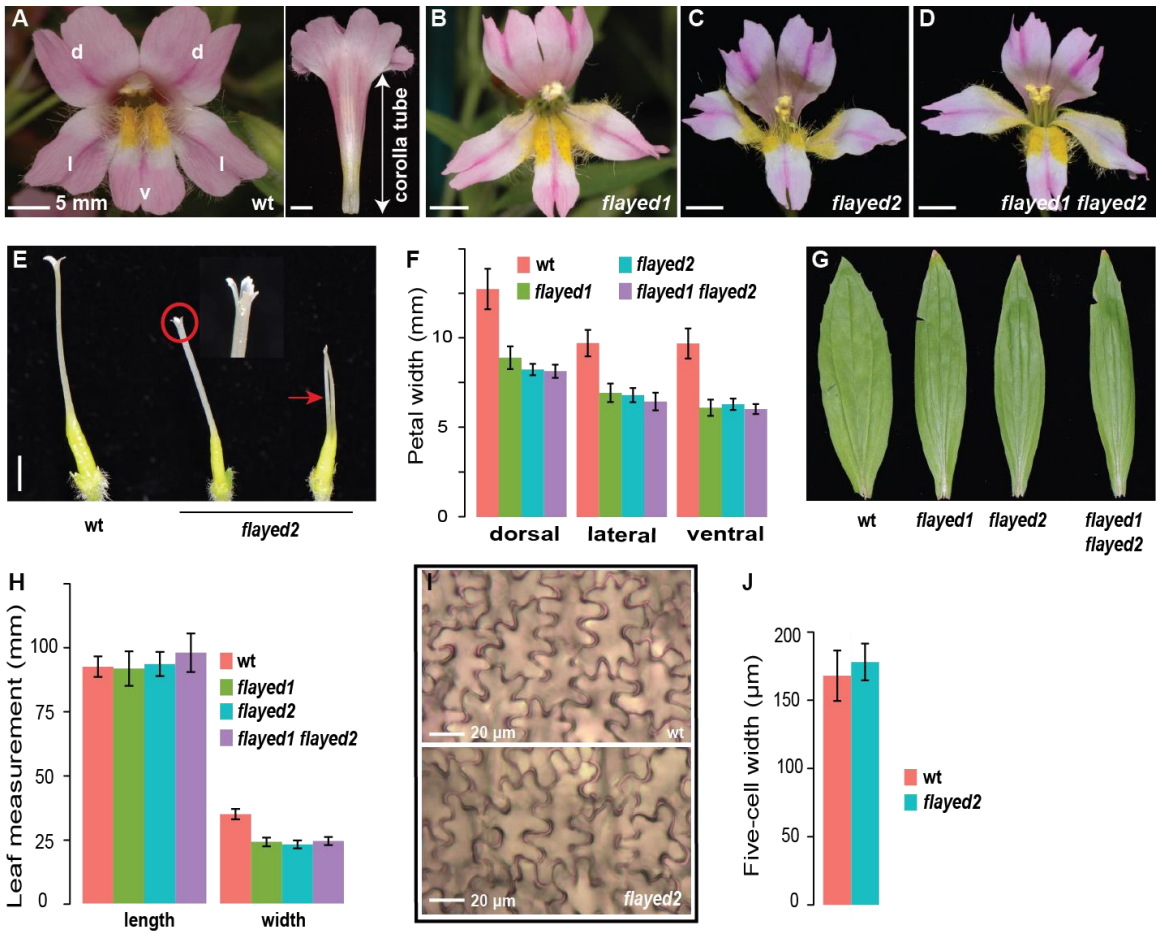

Fig. 1. Phenotypic characterization of the *flayed* mutants. (*A*) Front and back view of the *M. lewisii* (inbred line LF10) wild-type corolla. d: dorsal; l: lateral; v: ventral. (*B-D*) Front view of the corolla of *flayed1*, *flayed2*, and the double mutant. (*E*) Pistil of the wild-type (wt) and *flayed2*. The pistil phenotype of *flayed1* and the double mutant is the same as that of *flayed2*. (*F*) Quantitative comparison of petal width in wt (n =18), *flayed1* (n = 10), *flayed2* (n = 12), and the double mutant (n = 12). Detailed measurement data are presented in Table S1. (*G*) Overall shape of the fourth leaf (the largest leaf) of mature plants. (*H*) Quantitative comparison of length and width of the fourth leaf, with the same sample sizes as in (*F*). (*I*) Abaxial epidermal cells of dorsal petal lobes. (*J*) Width of five contiguous abaxial epidermal cells of the dorsal petal lobes in the wt (n = 15) and *flayed2* (n = 15). Error bars in (*F*), (*H*), and (*J*) are 1 SD.

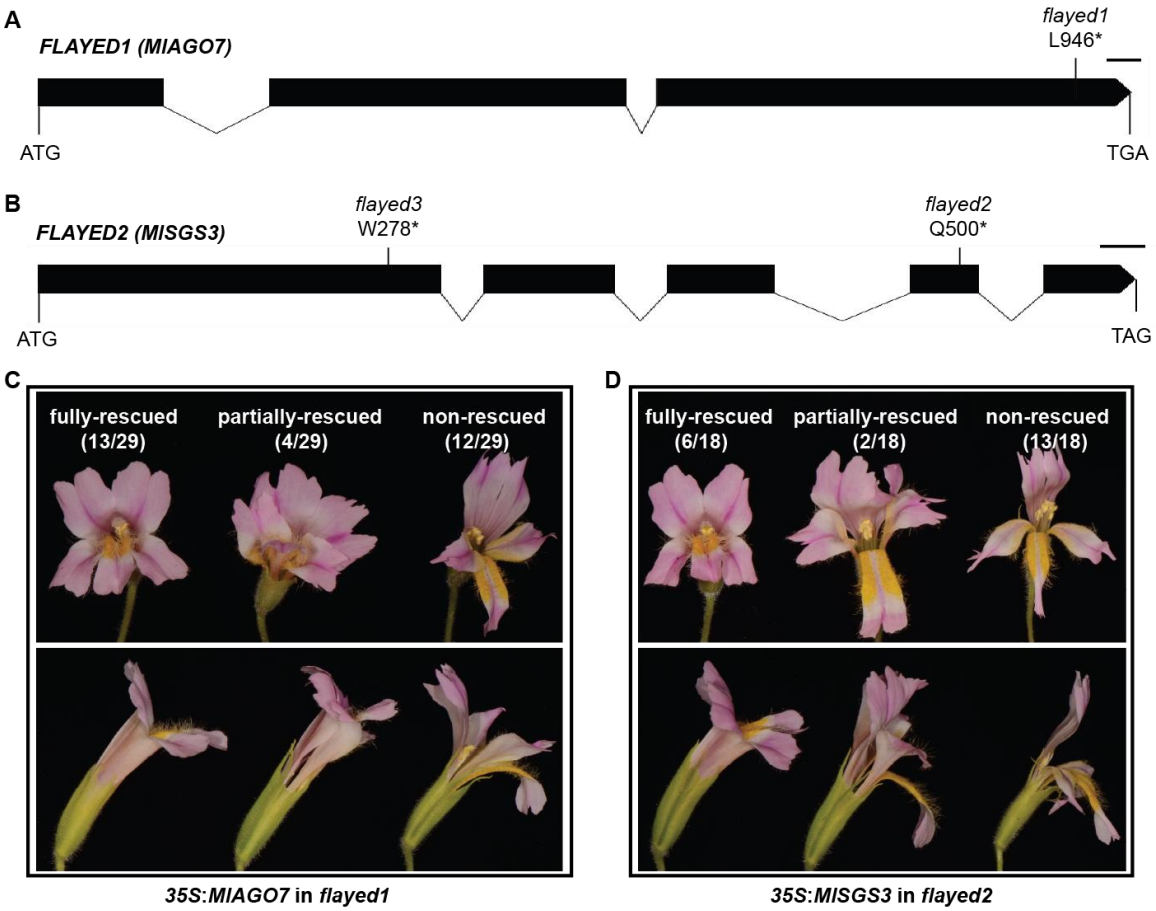

606

607 **Fig. 2.** *FLAYED1* and *FLAYED2* encode the orthologs of Arabidopsis AGO7 and SGS3,
608 respectively. (*A* and *B*) Schematics of *MlAGO7* and *MlSGS3* gene structure, with causal
609 mutations indicated. Black box: coding DNA; Line: Intron. Scale bars are 100 bp. (*C* and
610 *D*) Flower phenotypes of *35S:MlAGO7* and *35S:MlSGS3* transgenics in the *flayed1* and
611 *flayed2* mutant background, respectively (top: front view; bottom: side view). The
612 proportion of fully-rescued, partially-rescued, and non-rescued lines are shown in the
613 parentheses.
614

615

A

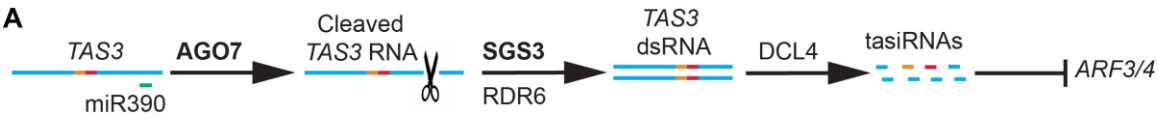

B

Sample	wt (a)	wt (b)	*flayed1* (a)	*flayed1* (b)	*flayed2* (a)	*flayed2* (b)
Total sRNA reads	11,425,515	16,447,166	18,199,489	15,869,380	15,861,817	18,443,718
All *TAS3L*-derived sRNA reads	5,780	10,319	171	172	160	162
tasiARF reads	104	224	1	1	0	1

Fig. 3. Small RNA analysis. (*A*) Schematic of the miR390-*TAS3*-*ARF* pathway. The orange and red lines represent the two tandem tasiARFs (see Fig. S2 for detailed annotations). (*B*) Small RNA counts in the wild-type (wt), *flayed1*, and *flayed2*. Two biological replicates were sequenced for each genotype.

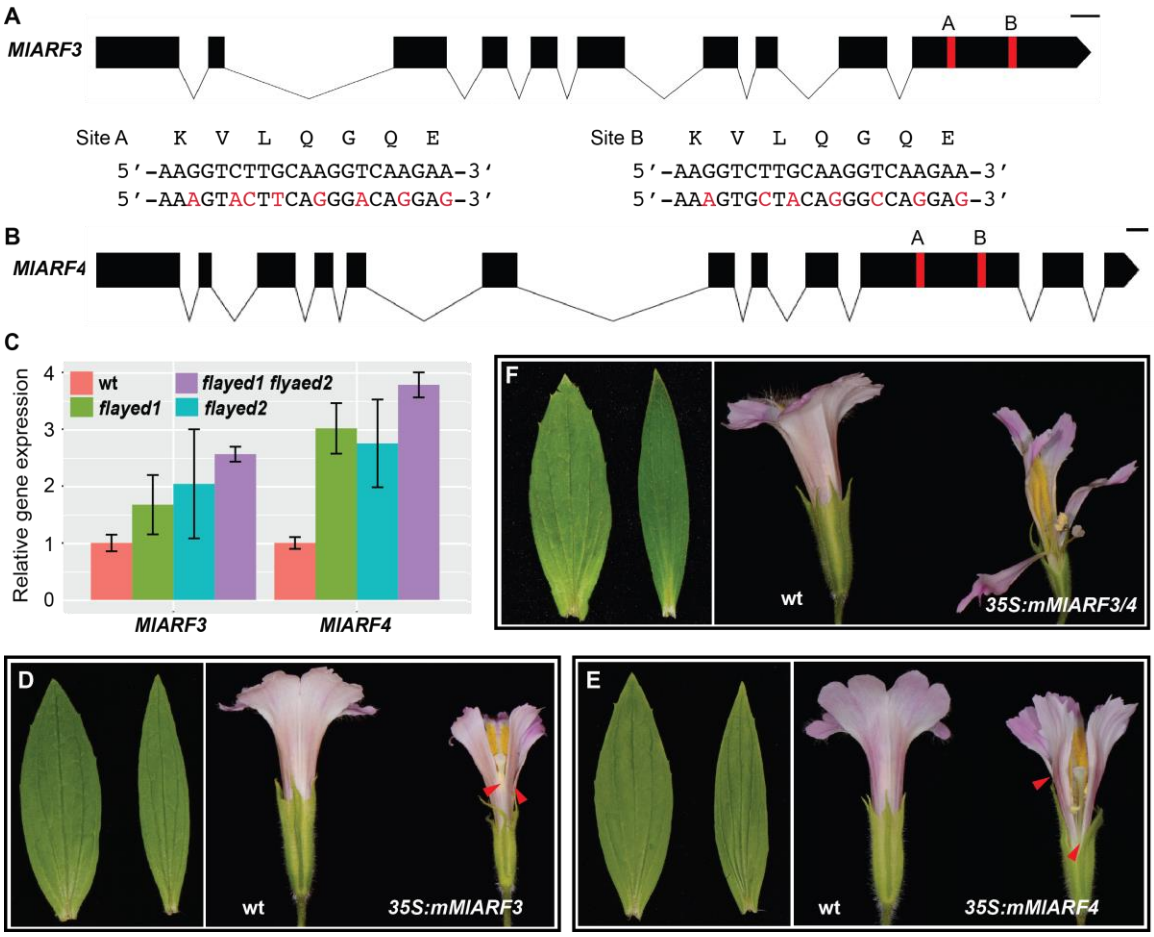

Fig. 4. The *flayed1/2* phenotypes are primarily mediated through up-regulation of *MlARF3/4*. (*A* and *B*) Schematics of *MlARF3* and *MlARF4* gene structure. Red bar: tasiARF binding site. Scale bars are 100 bp. The nucleotides highlighted in red are synonymous substitutions at the two tasiRNA binding sites that were introduced in the *35S:mMlARF3* and *35S:mMlARF4* constructs to circumvent tasiRNA repression. (*C*) Relative transcript level of *MlARF3* and *MlARF4* in 5-mm floral buds as determined by qRT-PCR. *MlUBC* was used as the reference gene. Error bars represent 1 SD from three biological replicates. (*D-F*) Leaf and flower phenotypes of strongest *35S:mMlARF3* (*D*), *35S:mMlARF4* (*E*), and double transgenic line (*F*). Left: wt; right: transgenic line. The red arrow heads indicate points of petal separation.

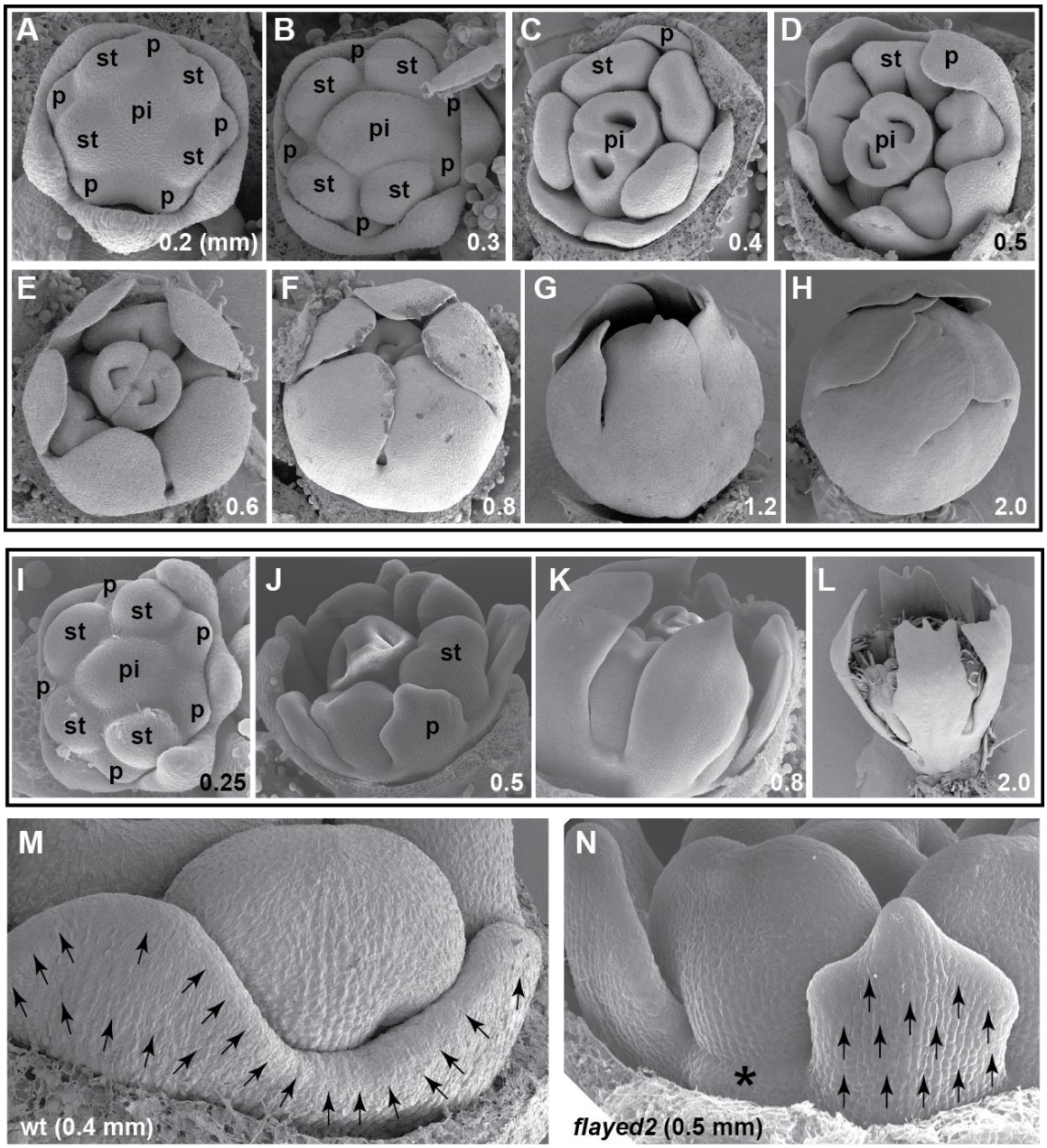

634

635

636 **Fig. 5.** Scanning electron micrographs of floral development. (*A-H*) *M. lewisii* wild-type
637 LF10. The developmental stages are marked on the bottom right of each image by the
638 diameter (in mm) of the corolla. From 0.4 mm onward, sepals were removed to show the
639 petals. (*I-L*) *flayed2*. (*M* and *N*) Detailed view of two adjacent petal primordia and the
640 inter-primordial region in the wt (*M*) and *flayed2* (*N*). Arrows indicate growth directions,
641 and the asterisk in (*N*) marks the arrested inter-primordial region. p = petal; st = stamen;
642 pi = pistil.
643

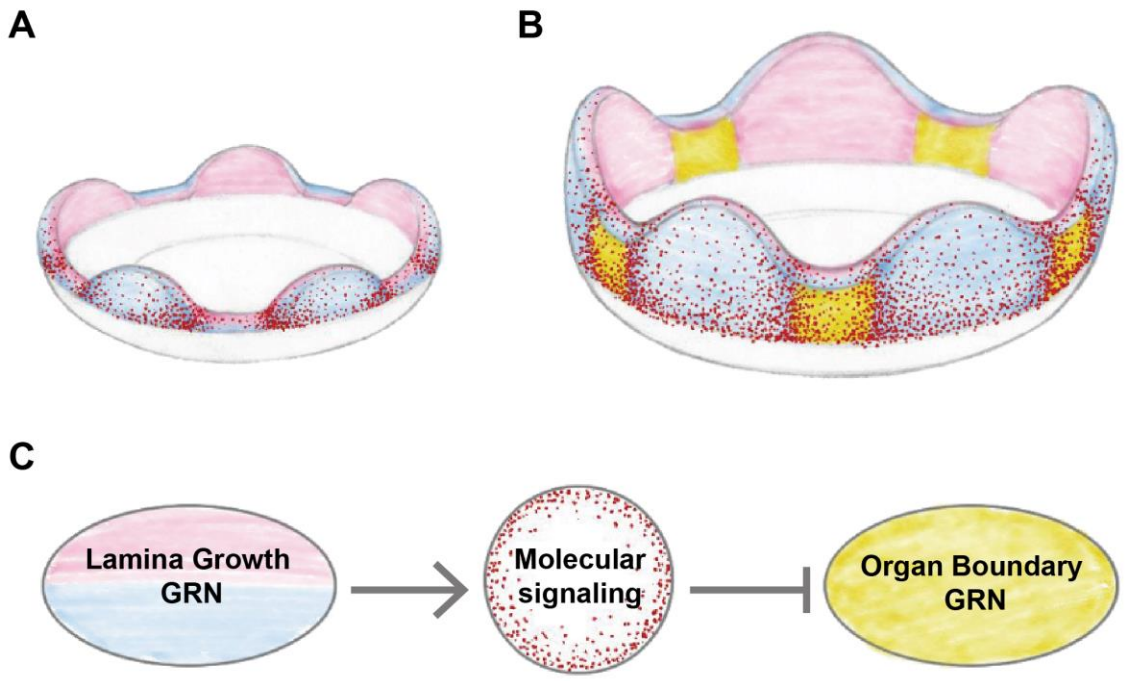

644

645 **Fig. 6.** A conceptual model for the developmental genetic control of corolla tube
646 formation in *Mimulus lewisii*. (*A*) Separate petal primordia at 0.3-mm (corolla diameter)
647 stage, when the hypothetical molecular signal (indicated by the red dots) starts moving
648 from the petal primordia to the inter-primordial regions. The pink and blue color indicates
649 the adaxial and abaxial side of the petal, respectively. (*B*) The molecular signal coming
650 from the petal primordia stimulates coordinated upward growth of the inter-primordia
651 regions (marked by the yellow color), resulting in congenital fusion of the petal primordia
652 by the 0.4-mm (corolla diameter) stage. (*C*) Relationships among the three modules.
653 GRN: Genetic Regulatory Network.
654

655 **Supporting Information**
656
657

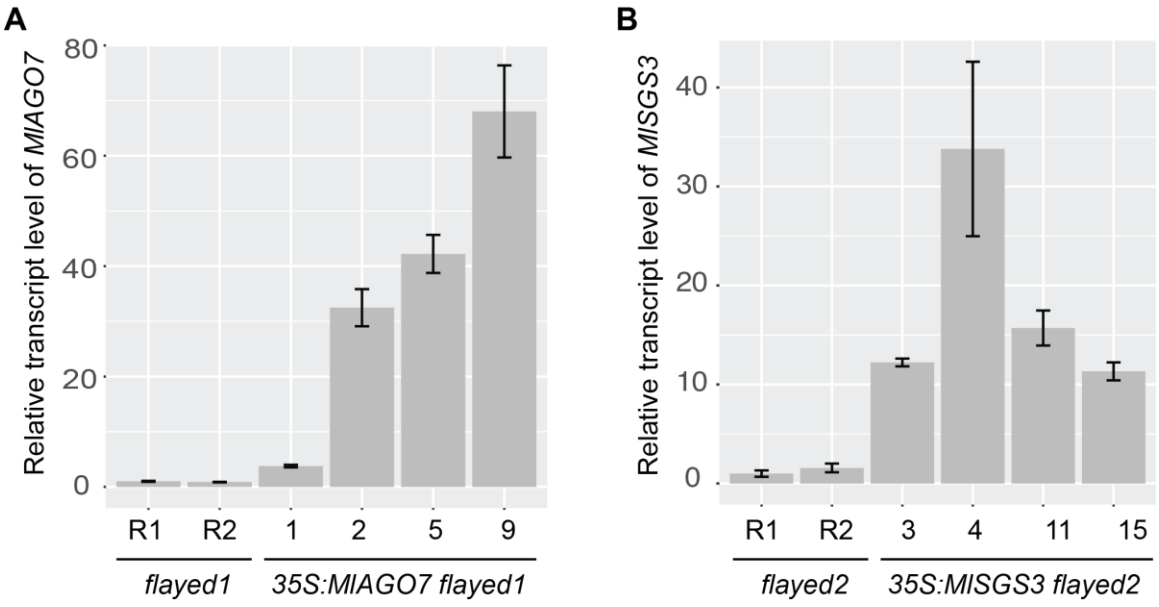

658
659
660 **Fig. S1.** Relative transcript level of *MlAGO7* (*A*) and *MlSGS3* (*B*) in 5-mm floral buds of
661 four representative, fully rescued over-expression lines compared to the corresponding
662 mutant backgrounds, as determined by qRT-PCR. R1 and R2 represent two biological
663 replicates. *MlUBC* was used as the reference gene. Error bars represent 1 SD from three
664 technical replicates.

665

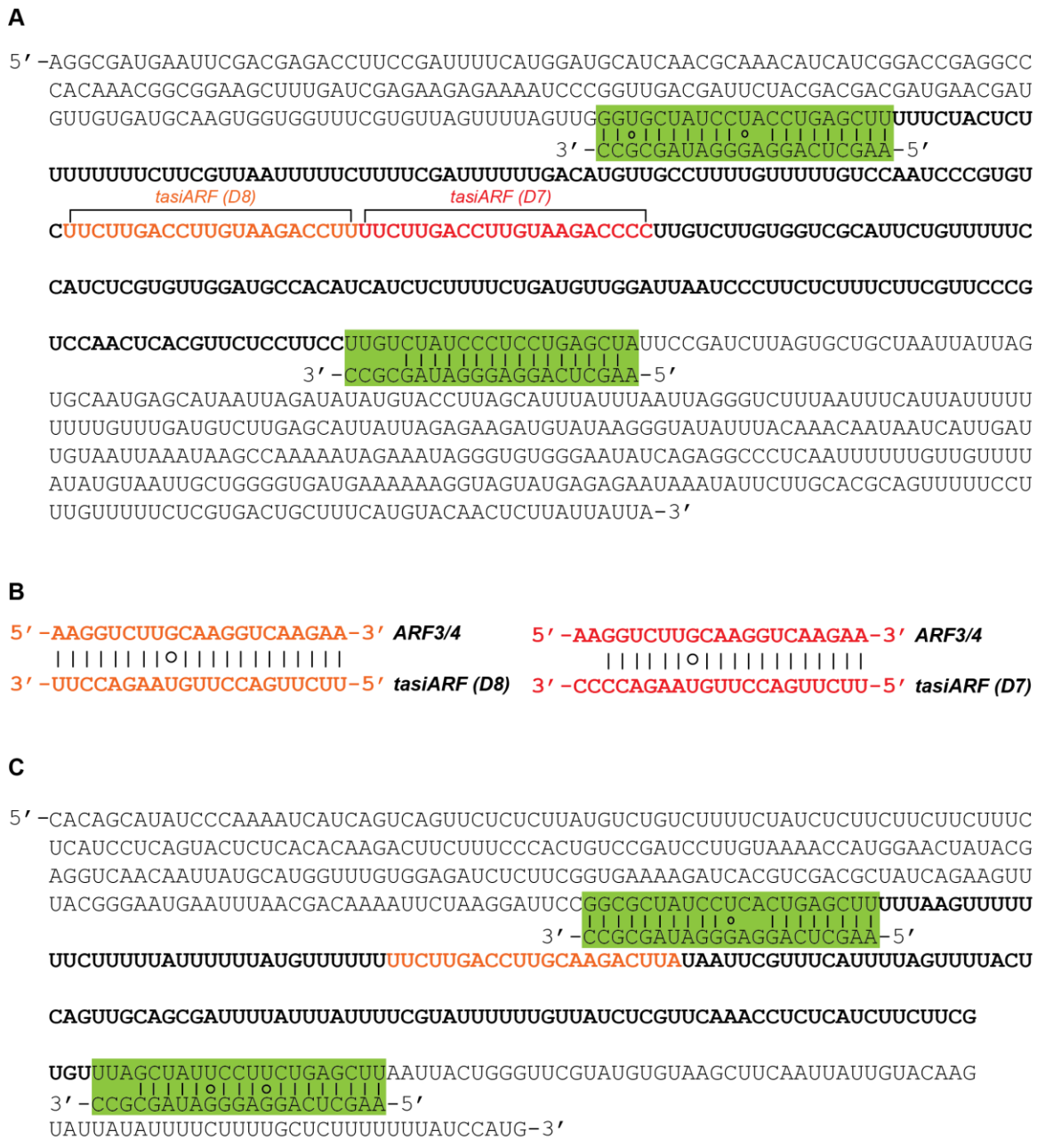

Fig. S2. Annotation of the *TAS3* transcripts in *Mimulus lewisii*. (*A*) *TAS3L*. The two miR390 binding sites are indicated by the green boxes; the tandem tasiARFs are highlighted in orange and red fonts. (*B*) Sequence complementarity between the two tasiARFs and the tasiARF-binding sites of *MlARF3/4*. (*C*) *TAS3S*. Highlighted are the miR390 binding sites and the single tasiARF sequence.

674

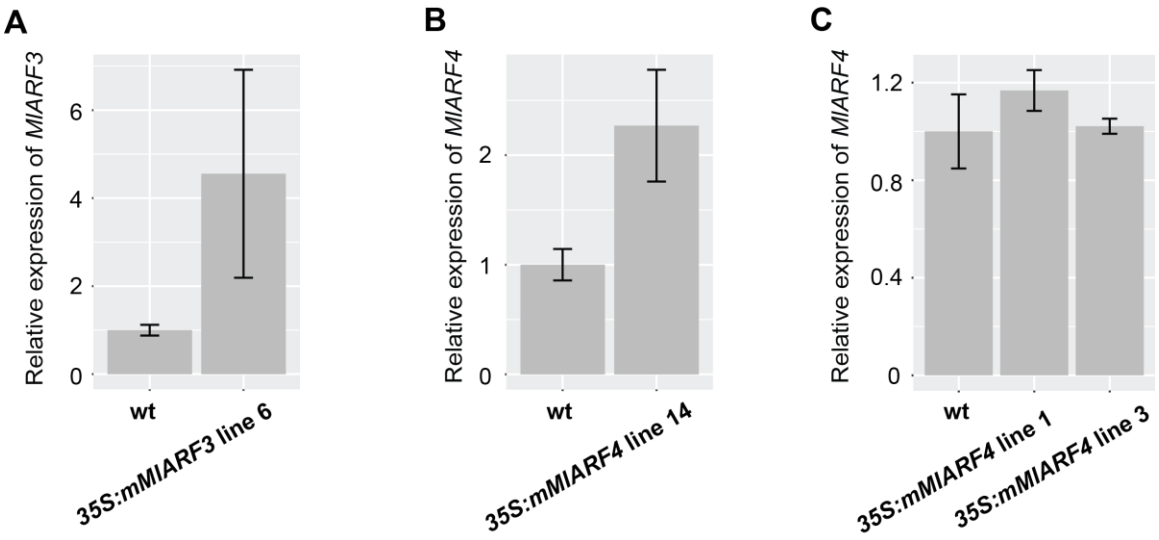

675

676 **Fig. S3.** Relative transcript level of *MlARF3/4* in 5-mm floral buds as determined by
677 qRT-PCR. (*A*) *MlARF3* in the *35S:mMlARF3* line with the strongest phenotype. (*B*)
678 *MlARF4* in the *35S:mMlARF4* line with the strongest phenotype. (*C*) *MlARF4* in two
679 *35S:mMlARF4* transgenic lines without any obvious phenotypes. *MlUBC* was used as the
680 reference gene. Error bars represent 1 SD from three biological replicates.
681

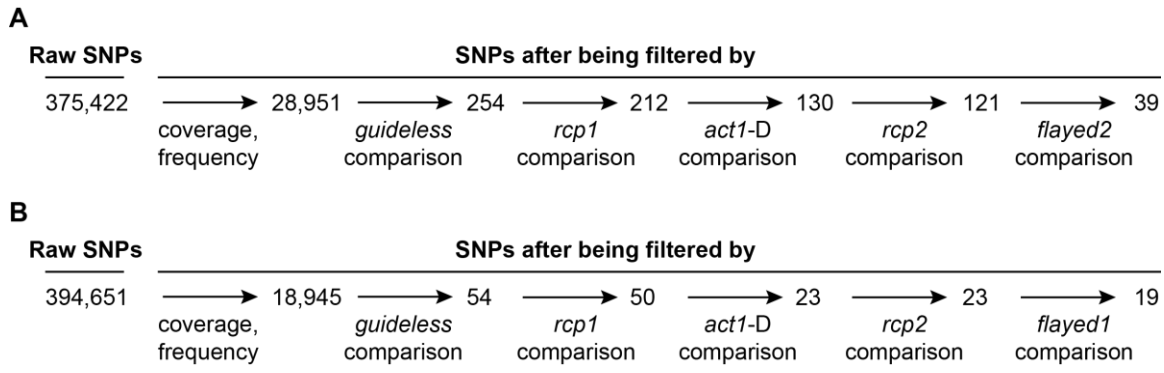

Fig. S4. SNP profile comparison between different EMS mutants. (*A*) Comparison between *flayed1* and other mutants. (*B*) comparison between *flayed2* and other mutants.

687 **Table S1.** Measurements of width (mm) of the dorsal, lateral and ventral petal, and the length
688 (mm) and width (mm) of the fourth leaf in *Mimulus lewisii* wild-type LF10 (n = 18), *flayed1* (n =
689 10), *flayed2* (n = 12) and the double mutant (n = 12) (mean±SD).
690

Trait	Wild-type	*flayed1*	*flayed2*	*flayed1 flayed2*
Dorsal Petal Width	12.71±1.13	8.88±0.63	8.23±0.32	8.13±0.37
Lateral Petal Width	9.7±0.73	6.92±0.51	6.80±0.39	6.44±0.49
Ventral Petal Width	9.68±0.84	6.1±0.45	6.29±0.32	6.02±0.28
Leaf Width	34.78±2.02	24±1.7	23±1.53	24.33±1.56
Leaf Length	92.31±4.02	91.6±6.74	93.33±4.70	97.75±7.5

691
692

693 **Table S2.** *FLAYED1* Candidate SNPs from the mutant genome comparisons. The SNP
694 highlighted in bold is the causal mutation.
695

LF10g_v1.8 scaffolds	Position	Wild-type	Mutant	Annotation
scaffold11	1859	C	T	Non-coding, repetitive sequence
scaffold24	263418	G	T	Non-coding, repetitive sequence
scaffold8	166102	T	A	Non-coding, repetitive sequence
scaffold52	174572	T	A	Non-coding sequence
scaffold52	288610	T	A	Non-coding, repetitive sequence
scaffold203	238265	A	T	Non-coding sequence
scaffold215	16351	G	A	Non-coding intergenic sequence
scaffold215	119479	C	T	Non-coding, repetitive sequence
scaffold215	252167	C	T	Non-coding, repetitive sequence
scaffold305	192826	T	C	Non-synonymous substitution at a non-conserved site of a mTERF domain-containing protein gene
scaffold319	280772	T	A	Non-coding, repetitive sequence
scaffold445	97914	T	A	Non-coding, repetitive sequence
scaffold462	69970	G	A	Non-coding, repetitive sequence
scaffold426	374050	A	G	Non-coding, repetitive sequence
scaffold450	155167	G	A	Non-coding sequence
scaffold399	668492	T	C	Non-coding, repetitive sequence
scaffold668	153018	G	A	LTR-retrotransposon
scaffold683	11631	C	T	Non-synonymous substitution at a non-conserved site of a PECTINESTERASE-related gene
scaffold564	125017	A	G	Intron of a SET-domain protein gene
scaffold564	334366	T	C	Non-coding sequence
scaffold836	462	G	A	Non-coding, repetitive sequence
scaffold965	79518	C	T	Non-coding sequence
scaffold1145	6875	C	T	Non-coding, repetitive sequence
scaffold1195	85177	G	A	Non-coding, repetitive sequence
scaffold1287	103555	G	A	Non-coding sequence
scaffold1294	57177	G	A	Non-coding, repetitive sequence
scaffold1315	55585	G	T	Non-coding, repetitive sequence
scaffold1584	**15734**	**A**	**T**	**Premature stop codon in *AGO7***

scaffold1617	13975	A	G	Non-coding, repetitive sequence
scaffold1605	96689	C	T	Non-coding, repetitive sequence
scaffold1734	37530	T	G	Non-coding, repetitive sequence
scaffold1746	13707	A	G	Non-coding, repetitive sequence
scaffold1789	71366	C	T	Non-coding, repetitive sequence
scaffold1885	24901	C	T	3'UTR of *Structural Maintenance of Chromosome 3* (*SMC3*)
scaffold1852	183687	G	A	Non-coding, repetitive sequence
scaffold2275	186058	C	T	Non-coding, repetitive sequence
scaffold2713	7833	G	A	Non-coding, repetitive sequence
scaffold3491	9533	C	T	Non-coding, repetitive sequence

696
697

698 **Table S3.** *FLAYED2* Candidate SNPs from the mutant genome comparisons. The SNP
699 highlighted in bold is the causal mutation.
700

LF10g_v1.8 scaffolds	Position	Wild-type	Mutant	Annotation
scaffold68	9337	T	C	Non-coding, repetitive sequence
scaffold156	**87555**	**G**	**A**	**Premature stop codon in *SGS3***
scaffold283	103550	T	A	Non-coding, repetitive sequence
scaffold249	427385	C	T	LTR-retrotransposon
scaffold432	106338	G	A	Non-coding, repetitive sequence
scaffold432	202697	A	T	Non-coding, repetitive sequence
scaffold427	215729	G	A	Non-coding, repetitive sequence
scaffold925	11368	C	T	Non-coding, repetitive sequence
scaffold1368	69701	G	A	Non-coding, repetitive sequence
scaffold1418	15654	T	A	Non-synonymous substitution at a non-conserved site of a calcium-dependent phospholipid-binding protein gene
scaffold1706	34503	C	T	Intron of a serine/threonine protein kinase gene
scaffold1884	10588	G	A	Non-coding, repetitive sequence
scaffold1977	48277	T	A	Non-coding, repetitive sequence
scaffold1987	42893	A	G	Non-coding sequence
scaffold1897	127158	A	G	Non-coding, repetitive sequence
scaffold2025	129655	T	A	Non-coding intergenic sequence
scaffold2466	11082	T	A	Mutator-like transposon
scaffold2643	10512	C	T	LTR-retrotransposon
scaffold2984	28110	C	T	Mutator-like transposon

701

702

703 **Table S4.** qRT-PCR Primers used in this study.
704

Gene	**Forward (5'-3')**	**Reverse (5'-3')**
MlAGO7	CGAGAATGAGGTCGCAAACTCA	AGCTTCAGCTTCGGAGGCTGAA
MlSGS3	GGACGACATTGATGACACTGA	AGGCTCGTTTATCTGCTCAACA
MlARF3	CGCAGCTCAGATATGCATGGAA	TGTCTCTTACAGCATGCCTGTC
MlARF4	GCGTGTTGTACACTGATAGCGA	CTTTGTGTCGTCGCTATTCATCC
MlUBC	GGCTTGGACTCTGCAGTCTGT	TCTTCGGCATGGCAGCAAGTC

705

706

707 **Table S5.** Primers used for plasmid constructions and sequence verification. The sequence
708 highlighted in red ("cacc") is the 4-bp sequence necessary for pENTR/D-TOPO cloning.
709

Primer	Sequence (5'-3')	Usage
*MlAGO7*_cdsF	caccATGGAAGAAGAAGAAGAAGGAAAG TCC	Plasmid construction& Sequencing
*MlAGO7*_SP1F	CCTCTGCATCTCACAGTTGCTC	Sequencing
*MlAGO7*_SP1R	GAGCAACTGTGAGATGCAGAGG	Sequencing
*MlAGO7*_SP2F	GCCGAAAGAACGAAGGGCTATTA	Sequencing
*MlAGO7*_SP2R	ATTACTGGGCGGACTAGCTACT	Sequencing
*MlAGO7*_Seq2F	TCCGGAAGATCATTCTACTCGA	Sequencing
*MlAGO7*_Seq2R	TCGAGTAGAATGATCTTCCGGA	Sequencing
*MlAGO7*_SP3F1	CGAGAATGAGGTCGCAAACTCA	Sequencing
*MlAGO7*_SP3R1	AGCTTCAGCTTCGGAGGCTGAA	Sequencing
*MlAGO7*_Seq3F	TTCTCGCGAATTTGGCTCTCA	Sequencing
*MlAGO7*_Seq3R	TGAGAGCCAAATTCGCGAGAA	Sequencing
*MlAGO7*_cdsR	GCAATAAAACATCAACTTGCTAATATTC	Plasmid construction & Sequencing
*MlSGS3*_cdsF	caccATGAGCTCAGGAAAAGGGATTGC	Plasmid construction & Sequencing
*MlSGS3*_seqF1	GGACGACATTGATGACACTGA	Sequencing
*MlSGS3*_seqR1	AGGCTCGTTTATCTGCTCAACA	Sequencing
*MlSGS3*_seqF2	CAGCAGTAGGATATGTAGAAGC	Sequencing
*MlSGS3*_seqR2	ATACGACCGCATCTCATACTTC	Sequencing
*MlSGS3*_cdsR	GTTGGATTTAGTTGGAGCGTAC	Plasmid construction & Sequencing
*MlARF3*_cdsF	caccATGATGTTCGGGTTAATCGATT	Plasmid construction & Sequencing
*MlARF3*_2F	GTTTCGCTAGTTCCAGATCAGCA	Sequencing
*MlARF3*_3R	GGAGTCATAGACTTTCCCATGC	Sequencing
*MlARF3*_10F	CGCAGCTCAGATATGCATGGAA	Sequencing
*MlARF3*_10R	TGTCTCTTACAGCATGCCTGTC	Sequencing
*MlARF3*_cdsR	CTACAGTGCTATATCAAGAAGCCT	Plasmid construction & Sequencing
*MlARF4*_cdsF	caccATGGGAATTATTGATCTGAATC	Plasmid construction & Sequencing
*MlARF4*_1F	TCCTCTGCTCTAACGTTTACTC	Sequencing

*MlARF4*_2F	TACACTCAGCTGAACCTGCTTC	Sequencing
*MlARF4*_2R	CTCTGATAGAGGAAGCAGGTTC	Sequencing
*MlARF4*_3R	TGAAGTCGACTTTGCAGGTGTA	Sequencing
*MlARF4*_6F	CAGAGTTCTTACCACAATGTCC	Sequencing
*MlARF4*_7R	TCTCAATCCAACAGGTATGCAG	Sequencing
*MlARF4*_9F	CATCTCTGAGCATCCAATCGTC	Sequencing
*MlARF4*_10R	AGATGTCCTGTCCGAAATCAGT	Sequencing
*MlARF4*_cdsR	TTAATCGGGCTGGCCCACAGAAGAT	Plasmid construction & Sequencing

710